Journal of Alloys and Compounds 607 (2014) 264–273

Contents lists available at ScienceDirect

Journal of Alloys and Compounds

journal homepage: www.elsevier.com/locate/jalcom

Critical current density of MgB_2 superconductor with (Bi,Pb)-2223 addition

D. Tripathi, T.K. Dey *

Cryogenic Engineering Centre, Indian Institute of Technology, Kharagpur 721302, India

ARTICLE INFO

Article history:
Received 10 March 2014
Received in revised form 7 April 2014
Accepted 8 April 2014
Available online 20 April 2014

Keywords:
(Bi,Pb)-2223 added MgB_2 superconductor
Solid state reaction
Magnetization
Critical current density
Scaling behavior
Collective pinning model

ABSTRACT

Polycrystalline MgB_2 pellets with and without addition of superconducting $Bi_{1.8}Pb_{0.26}Sr_2Ca_2Cu_3O_{10+x}$ powder has been synthesized by solid reaction. The effect of (Bi,Pb)-2223 addition on structural and critical current density of MgB_2 superconductor has been investigated. XRD data reveals no substitution for Mg or B. The superconducting transition temperature (T_{c0}) of MgB_2 (~37.97 K) remains almost invariant with 2223 addition. Temperature dependence of the normal state electrical resistivity of 2223 added MgB_2 is well explained by modified Rowell's model and it suggests that 2223 addition in MgB_2 marginally influences the percentage connectivity and intragrain residual resistivity. Critical current density (J_c) has been estimated at 4, 10, 20 and 30 K from M–H curves using Bean's model. MgB_2 sample with 1 wt.% of 2223 addition gives the best performance and display nearly two times enhancement in J_c compared to that of pure MgB_2 in the field range between 0 and ±6 T. Our analysis confirms that the observed magnetic field dependence of J_c of the present system is explained well in terms of the collective pinning model. Using the best fitted parameters (J_c (0) and H_0) of collective pinning model, an excellent scaling is established between the reduced critical current density, J_n (=J_o/J_c (0)) and the reduced field h_n (=H/H_0) at different temperatures for both pure and 2223 added MgB_2 polycrystalline pellets. It is also confirmed that δT_c type pinning dominates in pure MgB_2 and for 2223 added MgB_2 major contribution originates from δl type pinning at lower temperatures.

1. Introduction

A global interest in the field of superconductivity was generated by Nagamatsu et al. [1] with the discovery of superconductivity in an intermetallic compound MgB_2 in 2001. The reason behind the excitement was its high critical current density (J_c), absence of weak links, high superconducting transition temperature ($T_c \sim 39$ K), simple synthesis procedures and fairly low cost. These make MgB_2 a promising candidate for various superconductive devices operative at liquid hydrogen temperature. However, certain drawbacks, viz., sharp drop in J_c at high magnetic field, low irreversibility field (H_{irr}) and upper critical field (H_{c2}) limits the use of MgB_2 for practical applications. Chemical doping/addition [2–5], irradiation [6,7], and thermo-mechanical processing [8] are certain techniques those are used to overcome the above draw backs in MgB_2. Of these, chemical doping/addition proved to be an effective and a simple technique for improving the critical current density (J_c) of MgB_2 especially at high magnetic fields. Chemical doping is known to introduce inclusions as extra pinning centres, improves grain connectivity and enhances band scattering, which finally improves J_c of MgB_2 at high magnetic fields [9]. These extra pinning centres can either attract (in case of normal dopants) or repel (when superconductors with higher T_c are used as dopants) the flux lines in order to save core energy [10]. Most of the works so far on chemical doping in MgB_2 has been concentrated with addition of normal type of dopants. Consequently, the influence of addition of another superconductor with $T_c > 39$ K (viz., high temperature superconductors) on the superconducting properties of MgB_2 has been rather rare. To our knowledge, till date only a few reports are available on the influence of addition of high temperature superconductors (viz., YBCO, Bi-2212 and Bi-2223) in MgB_2 [11–13]. Rui et al. [11] was the first to investigate YBCO (nano) added MgB_2 superconductors and reported that (J_c–H) behavior for MgB_2 containing YBCO is inferior to that of pure MgB_2 and it becomes even poorer for higher doping level of 123. A preliminary report by Xu et al. [12] on the addition of both YBCO and Bi-2223 in MgB_2 indicates that J_c of 2223 added MgB_2 superconductor is superior to that obtained with addition of YBCO. Effect of addition of 2212 on the superconducting properties of MgB_2 superconductor has been reported by Shen et al. [13], which indicates appreciable improvement in J_c with the added

* Corresponding author. Tel.: +91 03222 283584; fax: +91 03222 282258.
E-mail address: tapasdey@hijli.iitkgp.ernet.in (T.K. Dey).

http://dx.doi.org/10.1016/j.jallcom.2014.04.057
0925-8388/

2212. Microstructural analysis clearly indicates the presence of significant amount of Bi-2212 particles in the MgB_2 matrix. It is important to note that all the above reports [11–13] confirms that T_c remains fairly invariant for both YBCO and BSCCO (2221 & 2223) added MgB_2, at least at fairly low concentration. It is known that addition of high T_c superconductor in MgB_2 introduces repulsive pins, which enhances the order parameter locally [10]. Brandt [14] and Thuneberg [15] analyzed the role of such inclusions of various shapes within the framework of both GL and BCS theories respectively. Repulsive pins are known to be less effective in pinning the flux line lattice (FLL) than the attractive pins, since the flux lines may flow around such pins. Brandt [10] concluded that if the pins are very dense such that their distance becomes $<\xi$ (coherence length), the notions repulsive and attractive lose their sense and the pinning potential becomes a 2D random function in each plane perpendicular to the flux lines.

Summing up, it is apparent that a detailed investigation on the superconducting properties (e.g. field dependence of J_c, pinning mechanisms, scaling behavior of J_c) of high temperature superconductors added MgB_2 has not been reported yet. In view of the above, the present report has been undertaken to investigate the effect of addition of 2223, on the field dependence of the critical current density (J_c) of MgB_2 superconductor. Magnetic field dependence of the critical current density of 2223 added MgB_2 polycrystalline pellets is discussed in light of various contemporary models to identify the pinning mechanisms operative in this system. We also confirm that critical current density of 2223 added MgB_2 display a new scaling.

2. Experimental details

Polycrystalline samples of MgB_2 with 0, 0.5, 1, 3 and 5 wt.% (Bi–Pb)-2223 addition are synthesized by conventional solid state reaction. The materials used as precursors are Mg (99%), amorphous B (200 mesh size) from M/S, Loba Chemicals (India). (Bi,Pb)-2223 superconducting powder ($T_C \sim 107$ K) is procured from M/S, Can Superconductors, Czech Republic. The composition of the superconducting powder is $Bi_{1.8}Pb_{0.26}Sr_2Ca_2Cu_3O_{10+x}$. The ingredients are well mixed in stoichiometric ratio in an agate mortar for three hours and are then pelletized in the form of cylindrical pellets of 15 mm diameter and ~3 mm thickness. The pellets are then placed in an alumina boat, which is positioned inside soft iron tube. The iron encapsulated pellets are heat treated at 775 °C for two and half hours in a programmable tubular furnace, under continuous argon flow at ambient pressure and are then slowly cooled to room temperature over a period of ~8 h.

Structural characterization of the prepared samples are carried out by XPERT-PRO diffractometer with a step size of 0.02 in the range of 20–70° using Cu Kα (λ = 1.5406 A°) target. The grain morphology of the prepared pellets is investigated using field emission gun scanning electron microscopy (FEG-SEM). Four probes dc resistivity measurement between 20 and 300 K is performed in a two stage cryocooler (APD, USA), using a Lakeshore model 331 PID temperature controller. Advantest TR-6142 current source is used to provide a constant current of 20 mA through the sample and a Keithley 2182 nano voltmeter is employed to read the sample voltage. The uncertainty in the resistivity measurement is estimated to be within ±1%. The magnetization measurement is carried out in an Evercool SQUID VSM (M/s, Quantum Design, USA) at four different temperatures (4, 10, 20 and 30 K) and for magnetic fields between ±6 Tesla with an accuracy of 10^{-8} emu. The bar shaped specimen with dimensions ~0.75 × 1.5 × 5 mm^3 and weight between 3 and 5 mg is used for magnetization measurement. The specimen is positioned in the sample holder such that the applied magnetic field is parallel to the sample length. DC magnetic moment is measured at 10 Oe between 15 and 50 K.

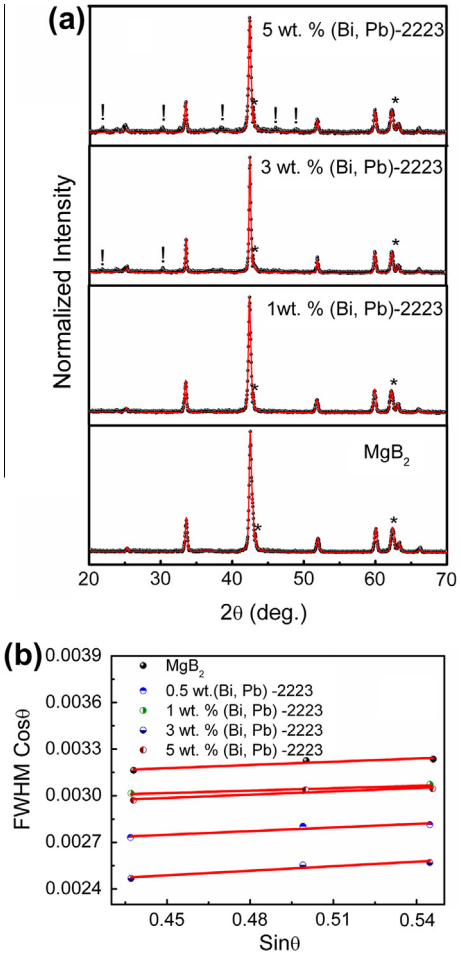

Fig. 1. (a) Rietveld refined XRD pattern of pure and 2223 added MgB_2 superconductor. (∗), and (!) represents reflections corresponding to MgO and (Bi,Pb)-2223 phase respectively. (b) Williamson–Hall plot for MgB_2 and 2223 added MgB_2.

3. Results and discussion

Fig. 1a shows the Rietveld refined XRD pattern of both pure and 2223 added polycrystalline MgB_2 pellets. Refinement is done by considering a small quantity of MgO impurity as secondary phase. In case of pure MgB_2, the refinement result confirms that except two small reflections of MgO (cubic structure with space group *Fm-3m*) at $2\theta = 42.96°$ and 62.4°, all other reflections correspond to hexagonal MgB_2 structure with *P6/mmm* space group. The volume fraction of MgO estimated from XRD pattern [16] is ~7% and is consistent with previous reports [17,18]. It may be noted that 2223 addition does not display any shift of the peak positions of MgB_2 and therefore, indicate no substitution for both Mg and B [19]. However, at higher level of 2223 addition ($\geqslant$3 wt.%), additional peaks corresponding to 2223 phase (JCPDS reference pattern

Table 1
Lattice parameters and their ratio, FWHM, Average crystallite size and Lattice strain of (Bi,Pb)-2223 superconductor added MgB_2 pellets.

(Bi,Pb)-2223 wt.%	$a = b$ (Å)	c (Å)	c/a	FWHM (°)			Average crystallite size (nm)	Lattice strain (%)
				[002]	[110]	[111]		
0	3.0852	3.5235	1.142	0.4034	0.4272	0.4428	48.31	0.069
0.5	3.0857	3.5247	1.142	0.3482	0.3708	0.3847	57.77	0.078
1	3.0856	3.524	1.142	0.3844	0.4011	0.4201	49.69	0.051
3	3.0857	3.5234	1.142	0.3145	0.3378	0.3514	67.63	0.097
5	3.0847	3.5221	1.142	0.3788	0.4020	0.4166	51.93	0.071

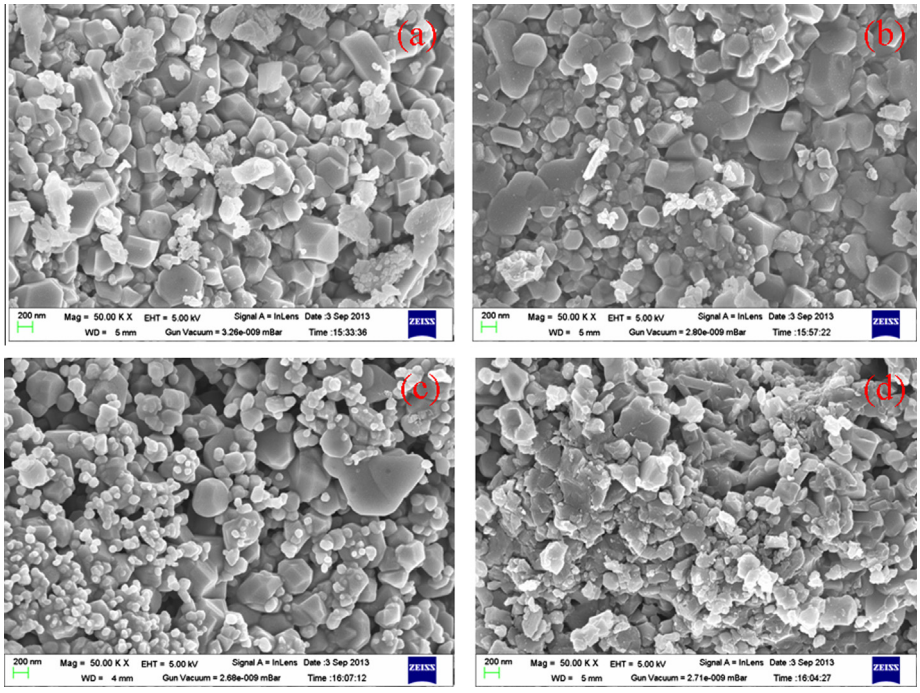

Fig. 2. FEG-SEM photographs of (a) MgB_2; (b) MgB_2 + 1 wt.% 2223; (c) MgB_2 + 3 wt.% 2223; and (d) MgB_2 + 5 wt.% 2223 polycrystalline pellets.

No. 80-1410; 80-2029) are revealed, which suggests the presence of 2223 grains or clusters. DTA analysis further confirms [20] that 2223 undergoes decomposition only at temperatures >800 °C under argon atmosphere. The lattice parameters estimated by Rietveld refinement for pure and 2223 added pellets is shown in Table 1. For pure MgB_2, the value of lattice parameter $a = b = 3.0852$ Å, and $c = 3.5235$ Å obtained in the present case are consistent with most of the earlier reports [21,22]. Table 1 indicates no significant change in lattice parameters and c/a ratio for 2223 added MgB_2 pellets and hence indicates absence of substitution effect. The Full Width at Half Maxima (FWHM) for the present set of samples for peaks (002), (110), and (111) are listed in Table 1. Williamson–Hall plot [23] for pure and 2223 added MgB_2 pellets in shown Fig. 1b. The lattice strain and the crystallite size estimated from WH plot are listed in Table 1. A small variation in both crystallite size and the lattice strain may be noted with 2223 loading in MgB_2, which accounts for marginal change in FWHM.

The morphological features of pure and 2223 added MgB_2 pellets are investigated by FEG-SEM and a few typical FEG-SEM photographs are shown in Fig. 2(a–d), which confirms hexagonal crystal structure of MgB_2 with randomly oriented grains of different size. For pure MgB_2 sample, grain size varies between 200 nm and 700 nm. Increasing 2223 content in MgB_2, shows the presence of 2223 clusters of various sizes distributed over the MgB_2 grains. EDAX analysis performed over a small surface area of 1 and 5 wt.% 2223 added MgB_2 pellets confirm presence of 2223 phase.

Fig. 3a shows the temperature dependence of the electrical resistivity of pure and 2223 added MgB_2. T_{c0} obtained from the resistivity data is found to be 37.97 K for pure MgB_2 samples and no significant change in T_{c0} of MgB_2 occur due to addition of 2223 superconductor (Table 2). Similar observations have also been reported earlier for both YBCO and 2212 added MgB_2 [11–13]. Temperature dependence magnetic response (ZFC) of the present samples between 15 K and 50 K are shown in Fig. 3b. The transition temperatures (T_c) obtained from M–T measurement shows a small decrease with increased content of 2223 in MgB_2 (Table 2). Fig. 3b reveals sharp superconducting transition up to 3 wt.% of 2223 added sample, while an increase in transition width is visible for 5 wt.% 2223 added MgB_2. The diamagnetic signal increases with addition of 2223, and reaches a maximum for 1 wt.% of 2223 addition; and with further increase in 2223 concentration in MgB_2, it decreases. This decrease in diamagnetic signal is attributed to the presence of weakly coupled grains in 2223 added samples [24].

The normal state electrical resistivity of the investigated samples is analyzed in terms of Rowell's approach [25] modified by Susner et al. [26] using Bloch–Gruneisen (B–G) function, which takes into account the role of porosity and intragrain connectivity in current transport. That is:

$$\rho_m(T) = F_{B-G}\left[\rho_0^i + \frac{k}{\theta_D}\left(\frac{T}{\theta_D}\right)^m \int_0^{\theta_D/T} \frac{e^x x^m}{(e^x-1)^2}\,dx\right] \quad (1)$$

Here, $\rho_m(T)$ is the measured resistivity between 40 and 300 K. ρ_0^i, m, θ_D and F_{B-G} are free parameters. The parameter 'm' is a number ranging between 3 and 5, while ρ_0^i, F_{B-G} and θ_D represent intragrain residual resistivity, resistivity enhancement factor and Debye temperature of polycrystalline samples respectively. The material parameter (k) has a value 0.0771 Ω cm K for MgB_2 [26] and it is assumed to be same for 2223 added MgB_2 pellets. The above equation is fitted with the experimental data (Fig. 3a) and the best fitted parameters are summarised in Table 2, along with the percentage connectivity (K_c) calculated using $K_c = 146/F_{B-G}$ [26]. It may be mentioned that in a polycrystalline sample, the connectivity primarily depends on several extrinsic microscopic artefacts, viz., porosity, polycrystalline anisotropy, intergrain boundaries and intergranular blocking phases, etc., [26]. In pure MgB_2, connectivity is essentially because of the presence of MgO formed at the edge of the MgB_2 grains and also those located in between the grains. In the present case, one can see (Table 2) that the connectivity decreases only marginally (~0.1%) for 0.5 wt.% addition of 2223, which indicates that compared to the pure MgB_2, the grain

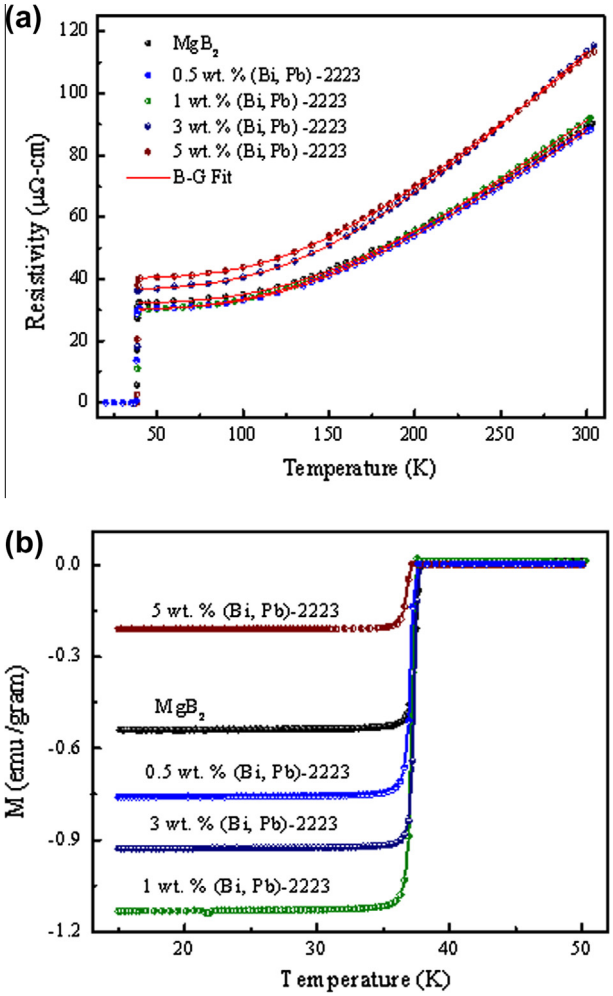

Fig. 3. (a) Temperature dependence of the electrical resistivity of pure and 2223 added MgB_2 pellets. Solid lines are the B–G Function Fit in normal state; (b) temperature dependence magnetic response of pure and 2223 added samples between 15 K and 50 K under 10 Oe magnetic field.

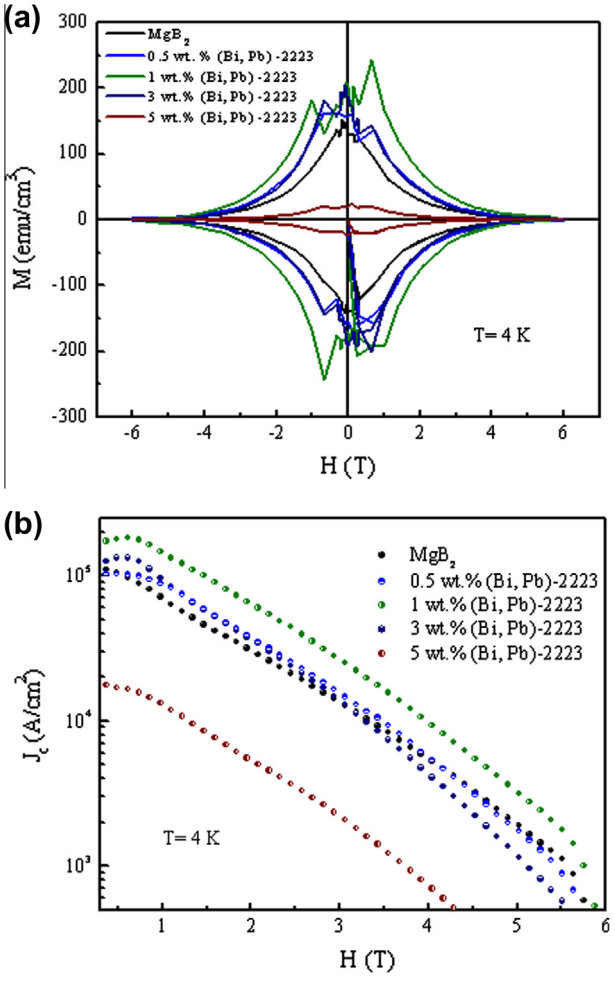

Fig. 4. (a) Typical (M–H) hysteresis loop for pure and MgB_2 containing 2223 superconductor measured at T = 4 K between 0 and ±6 T. (b) Critical current density (J_c) of pure and MgB_2 pellets containing 2223 estimated from the (M–H) curves measured at T = 4 K.

connectivity is not seriously affected with addition of 0.5 wt.% 2223. However, beyond 0.5 wt.% 2223, connectivity continues to decrease and attains a minimum for ~3 wt.% of 2223 addition in MgB_2. This decrease is attributed to the worsening of the intergrain connectivity due to the formation of Josephson junction weak links by granular 2223 located at the grain boundaries. However, at higher level of addition of 2223 (>3 wt.%), connectivity continues to improve appreciably. XRD data for sample with 2223 $\geqslant$ 3 wt.%, indicates presence of unreacted 2223 phase and the FEG-SEM pictures also confirms presence of 2223 superconducting clusters distributed over the surface of MgB_2 grains. It is known that the percolation threshold of conducting grains depends on the number of connections between nearest neighbours [27]. With increasing concentration of 2223 in MgB_2, the number of such connections between nearest neighbours enhances, which lowers the percolation threshold of the sample by providing a percolative path for the current transport [27]. Eisterer et al. [27] argued that the formation of such percolative paths reduces $\Delta\rho$ ($=\rho_{300}-\rho_{40}$) and enhances the connectivity of the sample, which is also observed in the present case (Table 2).

The (M–H) hysteresis loops for pure and 2223 added MgB_2 pellets are measured at different temperatures between 30 and 4 K in a magnetic field of ±6 T. Typical plots obtained for pure MgB_2 and 2223 added MgB_2 at 4 K are shown in Fig. 4a. An avalanche of flux is observed in the (M–H) loops, which is reproducible in both increasing as well as in decreasing magnetic field. Occurrence of such flux avalanche has been reported earlier in MgB_2, when local adiabatic conditions are fulfilled [28,29]. The inductive critical current density J_c (A/cm^2) is calculated from [30]:

Table 2
Superconducting transition temperatures (T_c) obtained from resistivity and magnetic measurement, residual resistivity (ρ_0^m), F_{B-G}, ρ_0^i, θ_D, m, $\rho(=\rho_{300}-\rho_{40})$ and K_c of pure and (Bi,Pb)-2223 added MgB_2 pellets.

(Bi,Pb)-2223 wt.%	T_{c0} (K) R–T	T_c (K) M–T	ρ_0^m (μΩ cm)	F_{B-G}	ρ_o^i (μΩ cm)	Θ_D (K)	m	$\Delta\rho$ (μΩ cm)	K_c (%)
0	37.97	36.65	32.14	11.42	2.83	1059.7	3.61	57.12	12.78
0.5	37.78	36.29	30.16	11.49	2.66	1050.9	3.54	57.32	12.70
1	37.99	36.31	29.86	12.24	2.46	1118.5	3.19	60.98	11.93
3	38.00	35.99	36.61	15.47	2.33	1084.2	3.41	76.70	9.44
5	38.01	35.97	39.75	13.75	2.93	1021.5	3.61	71.88	10.62

$$J_c = \frac{20\Delta M}{a(1 - a/3b)} \quad (2)$$

where $\Delta M = M^+ - M^-$ is the width of magnetization loop, a and b ($a < b$) are the cross-sectional dimensions of the sample perpendicular to the applied magnetic field.

Fig. 4b shows the calculated J_c as a function of applied field for pure and 2223 added MgB_2 pellets at 4 K. The field dependent critical current density (J_c) of the present MgB_2 agrees fairly well with the reports on samples prepared by similar technique [31,32]. The optimal concentration of 2223 in MgB_2 for which J_C is maximum and is nearly 2 times higher than that of pure MgB_2 over both low and high field region, appears to be 1 wt.% of 2223. This enhancement in J_c is comparable to that reported by Shen et al. [13] for their 3 wt.% 2212 added MgB_2 pellets. It is important to note that an improvement in J_c is also seen in 0.5 wt.% and 3 wt.% 2223 added MgB_2 samples at low fields. However, for 3 wt.% 2223 added MgB_2 sample for field >3T, the critical current density slowly drops below that for pure MgB_2, while for sample containing 0.5 wt.% 2223 beyond 3T, J_c follows that for pure MgB_2. Addition of 2223 ($\geqslant$5 wt.%) in MgB_2 reduces J_c significantly in both low and high field regions. Such behavior in J_c has been reported earlier in MgB_2 and is believed to originate from the counterbalancing effect [33] of nanometric inhomogeneity and suppression of matrix superconductivity caused by 2223 addition.

Generally $H_{irr}(T)$ is defined as the crossover field separating the solid vortex region into liquid vortex region. In other words $H_{irr}(T)$ is the field above which the depinning of vortex starts, while $H_{c2}(T)$ is the crossover field between superconducting and normal state of the superconductor. In low temperature superconductor these two fields are nearly same and hence $H_{c2}(T)$ is usually used as scaling field. However, for intermediate and high temperature superconductors this liquid vortex region exists and therefore, pinning force cannot be defined above the depinning line (viz., above $H_{irr}(T)$). Therefore, in these class of superconductors, irreversible field ($H_{irr}(T)$) is widely used as the scaling field in place of $H_{c2}(T)$ [34]. In order to explore J_c–H behavior of 2223 added MgB_2, the irreversible field (H_{irr}) for the present set of samples are estimated using Kramer plot (viz., $J_c^{0.5} H^{0.25}$ *vs.* H) at different temperatures. H_{irr} is estimated by extrapolating the linear part of the Kramer plot up to the field for which $J_c^{0.5} H^{0.25}$ goes to zero [35,36]. Fig. 5a represents a typical such plot for the present set of samples at 4 K. The irreversible field (H_{irr}) estimated for pure MgB_2 pellets compares fairly well with the reported values [37] and H_{irr} of 2223 added MgB_2 pellets estimated at different temperatures are found to be nearly constant (Fig. 5b). Several theoretical models have been proposed over the years, to account for the field dependence of critical current density of superconductors. In the following section, we discuss our results on the field dependence of J_c of pure and 2223 added MgB_2 pellets in light of some of the relevant models. One of the earliest models very widely used to account for the field dependence of J_c, was proposed by Kramer [36], which is based on the interactions of the flux line lattice with the grain boundaries or planer dislocations and is given as:

$$J_c(h) = J_0(h)^{-0.5}[1 - h]^2 \quad (3)$$

J_0 and h in Eq. (3) represent zero field J_c and the reduced field ($h = H/H_{irr}$) respectively. For a two band superconductor, like, MgB_2, Wang et al. [38] argued that at high magnetic fields due to smaller energy gap and strong pair breaking, the order parameter of π band is suppressed rapidly. Thereby, the critical current density of MgB_2 is shared between π and σ bands and accordingly Wang et al. [38] proposed:

$$J_c(H) = J_{01}\exp(-10H/H_{c2}) + J_{02}\exp(-2.2H/H_{c2}) \quad (4)$$

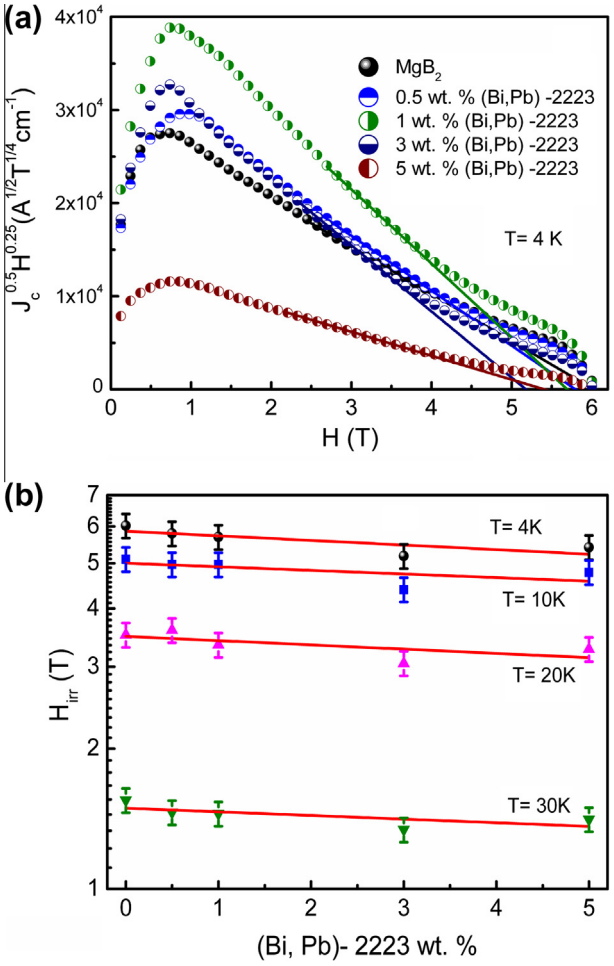

Fig. 5. (a) A typical plot of $Jc^{0.5}$ $H^{0.25}$ as a function of H to calculate the irreversible filed (H_{irr}) of MgB_2 and MgB_2 containing various amounts of 2223 at $T = 4$ K; (b) irreversible filed (H_{irr}) for pure and 2223 added MgB_2 pellets plotted as a function of 2223 wt.% at different temperatures. Solid line shows the linear fit of H_{irr} data.

where J_{01}, J_{02} and H_{c2} are zero field J_c of the two bands and upper critical field respectively. Influence of porosity and agglomeration on J_c of MgB_2 superconductor was considered by Horvat et al. [39] to derive the field dependence of critical current density. They assumed that MgB_2 cells are surrounded by voids and are connected by narrow bridges. In such a scenario, the superconducting screening current on whole sample flows only if the screening current can pass through these bridges connecting the cells. As the area for screening current in the bridge is small, the current density in the bridges is larger than that in the cells. However, in order to make the net current density in the cells same as the current density J_c, additional current screening on the length scale of the cells is needed. Consequently, in addition to screening around the whole sample, the superconducting screening current also flows on two different length scales and percolate between the voids in the ensuing structure. The two different superconducting screening currents have different contributions to the measured magnetic moment and consequently critical current density. Horvat et al. [39] deduced the field dependence of J_c as a stretched exponential function as:

$$J_c(H) = \alpha \exp\left(-\left(\frac{H}{H_1}\right)^{n1}\right) + \beta \exp\left(-\left(\frac{H}{H_2}\right)^{n2}\right) \quad (5)$$

In Eq. (5), both α and β are fitting parameters, which accounts for the relative contribution of each of the screening currents. The parameters H_1, H_2, $n1$, and n2 are estimated from the double

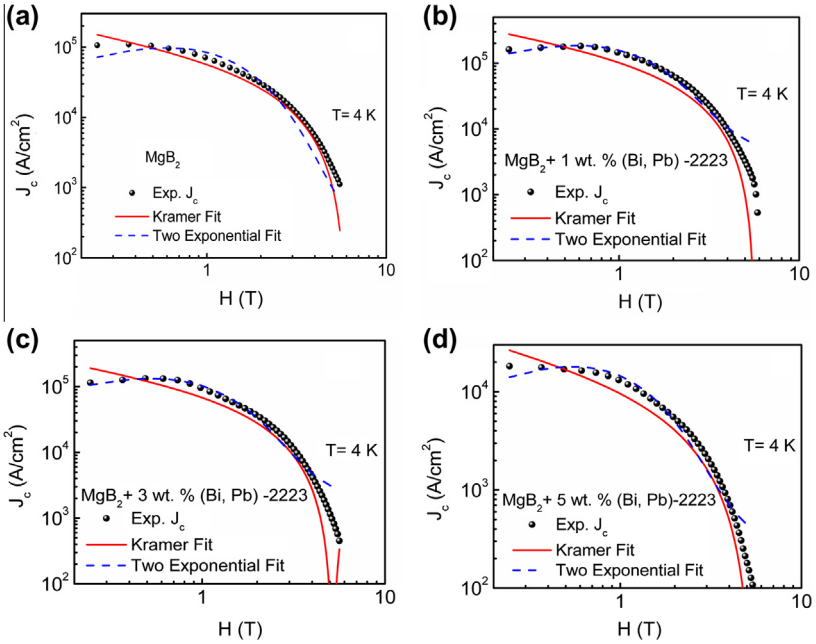

Fig. 6. Typical plots of the critical current density (J_c) for (a) MgB_2; (b) MgB_2 + 1 wt.% 2223; (c) MgB_2 + 3 wt.% 2223; and (d) MgB_2 + 5 wt.% 2223 pellets at 4 K. Solid lines are the fitted J_c by Kramer (solid line) and two exponential (dashed line) model.

logarithmic plot of $-d[ln(\Delta m)]/dH$ *vs.* H and are related to sample properties. The values of H_1 and H_2 depend on the quality and the temperature of the sample; better the quality of samples higher are the values of H_1 and H_2 (for MgB_2 at 20 K, H_2 ~2.5 T and is always larger than H_1). $n1$, and $n2$ typically lie in the range between 2.2–3.2 and 2.4–2.9 respectively [39].

Lastly, based on the assumption that the disorders or defects present in the samples leads to the formation of vortex lattice, Blatter et al. [40] proposed the 'collective pinning model' and defined four regimes: single vortex, small bundle, large bundle and vortex liquid region. These regions are separated by crossover field and show different J_c *vs.* H behavior. The field separating the 'single vortex region' and 'small bundle region' is known as 'crossover field' (H_{sb}). In the 'small bundle region' ($H_{lb} \leqslant H > H_{sb}$), the critical current density (J_c) behaves as [40]:

$$J_c(H) = J_c(0)\exp\left[-(H/H_0)^{3/2}\right] \quad (6)$$

where $J_c(0)$, H_0 and H_{lb} are the zero field J_c, normalization field and the crossover field separating small and large bundle region respectively. In the region, $H > H_{lb}$ (viz., 'large bundle region'), J_c follows a power law of the type: $J_c(H) \propto H^{-3}$.

The field dependent J_c of pure and 2223 added MgB_2 pellets are analyzed in the light of the above referred models [36,38–40]. It is clear from Fig. 6(a–d) that Kramer model [36] completely fails to account the field dependence of J_c of pure and 2223 added MgB_2 samples. Though the quality of fit of J_c–H data in case of two exponential model [38] is little better than the Kramer model, it significantly deviates both at low and high magnetic fields. In order to examine the present set of data in light of Eq. (5), the sample dependent parameters, viz., H_1, H_2, $n1$, and $n2$ are first calculated from the measured field dependence of ΔM of both pure and 2223 added MgB_2 samples, following the procedures adopted by Horvat et al. [39], viz., from the linear part of log–log plots between $-d[ln(\Delta m)]/dH$ and H. A typical plot of $-d[ln(\Delta m)]/dH$ as function of the magnetic field for pure MgB_2 is shown in Fig. 7a. For the pure and 2223 added MgB_2 pellets at various temperatures (viz., 4, 10, 20 and 30 K), the value of H_2 lies between 1.0 and 4.49 T and is always larger than H_1 (Table 3). The calculated values of $n1$, and $n2$ for the present samples are in the range of 1.29–2.65 and 1.36–2.79, respectively. Finally, using the estimated values of H_1,

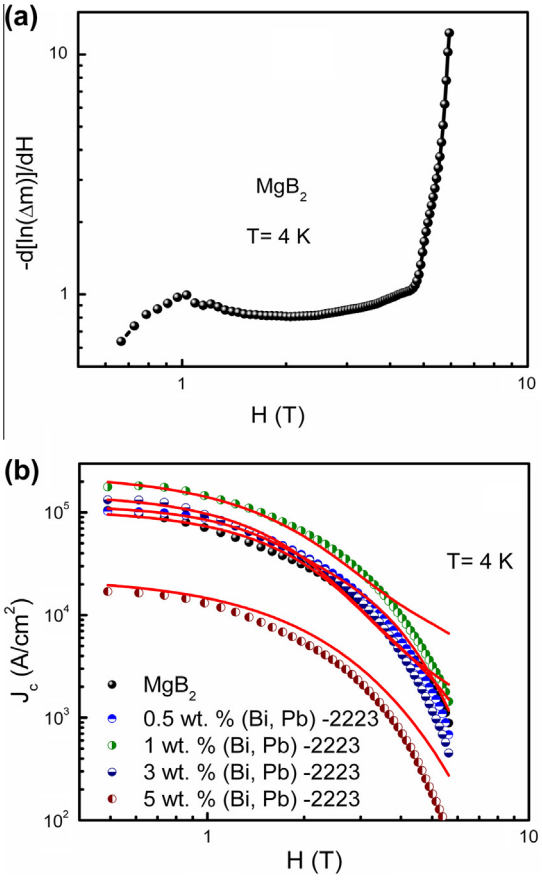

Fig. 7. (a) Typical plots showing the variation of $-d[ln(\Delta m)]/dH$ with applied magnetic field for MgB_2 at 4 K; (b) field dependent J_c of pure and 2223 added MgB_2 samples fitted by Horvat (solid lines) model at T = 4 K.

Table 3
Calculated values of parameters H_1, n_1, H_2, n_2 along with the fitted parameters α and β used in stretched exponential function proposed by Horvat et al. [38] at 4 and 20 K respectively.

(Bi,Pb)-2223 wt.%	4 K						20 K					
	H_1	H_2	n_1	n_2	$\alpha * 10^4$	$\beta * 10^4$	H_1	H_2	n_1	n_2	$\alpha * 10^4$	$\beta * 10^4$
0	1.67	1.49	1.91	1.72	9.90	0.83	1.10	1.57	1.74	2.79	5.65	1.66
0.5	1.35	2.59	2.35	1.72	5.61	6.11	1.19	1.71	2.25	1.71	6.34	1.78
1	1.45	4.70	1.51	1.36	21.20	2.44	1.62	1.83	1.60	1.65	13.28	0.49
3	1.47	2.92	1.79	1.51	12.95	2.23	1.47	1.49	1.60	1.79	0.5	6.68
5	1.50	2.69	1.42	1.61	1.82	0.51	1.07	1.95	3.97	1.45	0.74	0.52

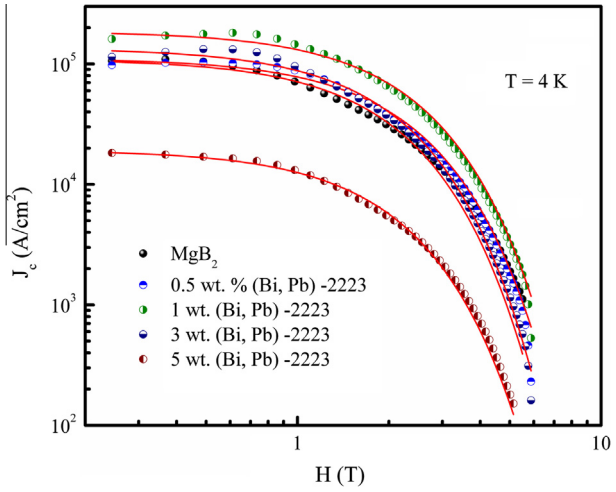

Fig. 8. Typical plots of the critical current density (J_c) as a function of H for MgB_2 and MgB_2 containing various amounts of 2223. Solid lines represents the Blatter fit (Eq. (6)) at $T = 4$ K.

H_2, $n1$, and $n2$, the measured J_c is fitted with Eq. (5) taking both α and β as free parameters. Typical results for all the samples at 4 K are shown in Fig. 7b. The best fitted values of α and β, along with the calculated values of H_1, H_2, $n1$, and $n2$ are given in Table 3 for 4 K and 20 K. It is clearly apparent from Fig. 7b that the agreement of the present data with Eq. (5) proposed by Horvat et al. [39] is far from satisfactory. To our knowledge, for bulk MgB_2 only report available till date in support of the proposition suggested by Horvat et al. [39] is by Sudesh et al. [41]. They, however, demonstrated fair correspondence between the measured field dependence of the pinning force density of MgB_2 with that estimated by Horvat model, taking all the six parameters (viz. α, β, H_1, H_2, $n1$, and $n2$) as free parameters. Therefore, the validity of their results is questionable due to the use of as many as 'six' adjustable parameters.

On the contrary, it may be noted that Eq. (6) derived using 'collective pinning model' [40] explains very well, the measured field dependence of critical current density of both pure and 2223 added MgB_2 pellets at different temperatures. A typical plot of the measured J_c *vs.* H dependence for both pure and 2223 added MgB_2 samples at 4 K with the Blatter's Eq. (6) is shown in Fig. 8. A small deviation in J_c estimated by collective pinning model seen both at low and high magnetic fields are expected due to applicability of Eq. (6) only in the intermediate field region, where vortex pinning occurs in the form of small bundles [42,43]. The double logarithmic plot between $-\log\{J_c(H)/J_c(0)\}$ *vs.* H shows deviation at both low as well as high field and is generally used for estimation of the cross over field (H_{sb}). A typical such plot for MgB_2 + 1 - wt.% 2223 sample is shown in Fig. 9a and b shows the crossover fields (H_{sb}) of 2223 added MgB_2 samples as a function of the reduced temperatures ($t = T/T_c$). The crossover fields (H_{sb}) along with the best fitted parameters $J_c(0)$, H_0 of Eq. (6) at different temperatures are listed in Table 4 for both pure and 2223 added MgB_2.

To the best of our knowledge, reports on the observation of scaling of J_c of MgB_2 superconductors with respect to magnetic field are not many [44,45], though there are instances of such scaling for conventional superconductors [46,47]. Normalized critical current density ($J_c/J_{c,max}$) of neodymium based superconductors [46] was reported to scale with h_p ($hp = H/H_p$), where H_p is the field corresponding to $J_{c,max}$. Similarly, critical current density of lutetium based superconductor [47] has been demonstrated to scale with thermodynamic critical field (H_c) as the normalization factor. It is

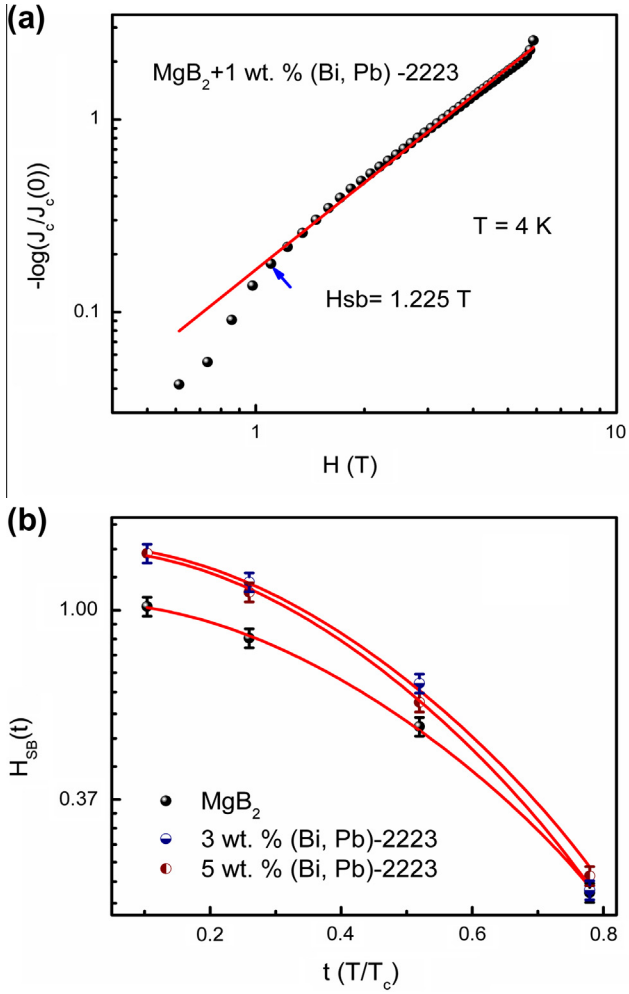

Fig. 9. (a) Double logarithmic plots of $-\log(J_c/J_c(0))$ as a function of H for 1 wt.% 2223 added MgB_2 pellet at T = 4 K. The solid represents the Blatter fit in small bundle region. (b) Plot of the crossover field (H_{SB}) as a function of reduced temperature (t) for pure MgB_2 and MgB_2 containing 3 wt.% and 5 wt.% 2223. The solid lines are the H_{SB} fitted using Eq. (9).

Table 4
The value of different fitted parameters viz. J_c (0), H_o, crossover field H_{sb} and P_1 for investigated samples at different temperatures.

(Bi, Pb) 2223 wt.%	4 K				10 K			20 K			30 K			
	$J_c(0) * 10^5$ A/cm^2	H_o (T)	H_{sb} (T)	$J_c(0) * 10^5$ A/cm^2	H_o (T)	H_{sb} (T)	$J_c(0) * 10^5$ A/cm^2	H_o (T)	H_{sb} (T)	$J_c(0) * 10^4$ A/cm^2	H_o (T)	H_{sb} (T)	P_1	H_{sb} (0) (T)
0	1.09	1.74	1.02	1.04	1.57	0.863	0.824	1.13	0.541	1.52	0.539	0.225	0.504	1.959
0.5	1.12	1.97	1.35	1.30	1.55	1.11	1.01	1.09	0.631	4.12	0.525	0.245	0.453	1.378
1	1.87	1.99	1.225	1.90	1.72	1.06	1.72	1.12	0.613	8.08	0.513	0.245	0.416	1.37
3	1.35	1.74	0.987	1.39	1.44	0.627	0.972	1.09	0.68	4.48	0.494	0.192	0.385	1.407
5	0.194	1.74	0.367	0.229	1.36	0.61	0.177	0.960	0.43	0.73	0.453	0.176	0.331	1.378

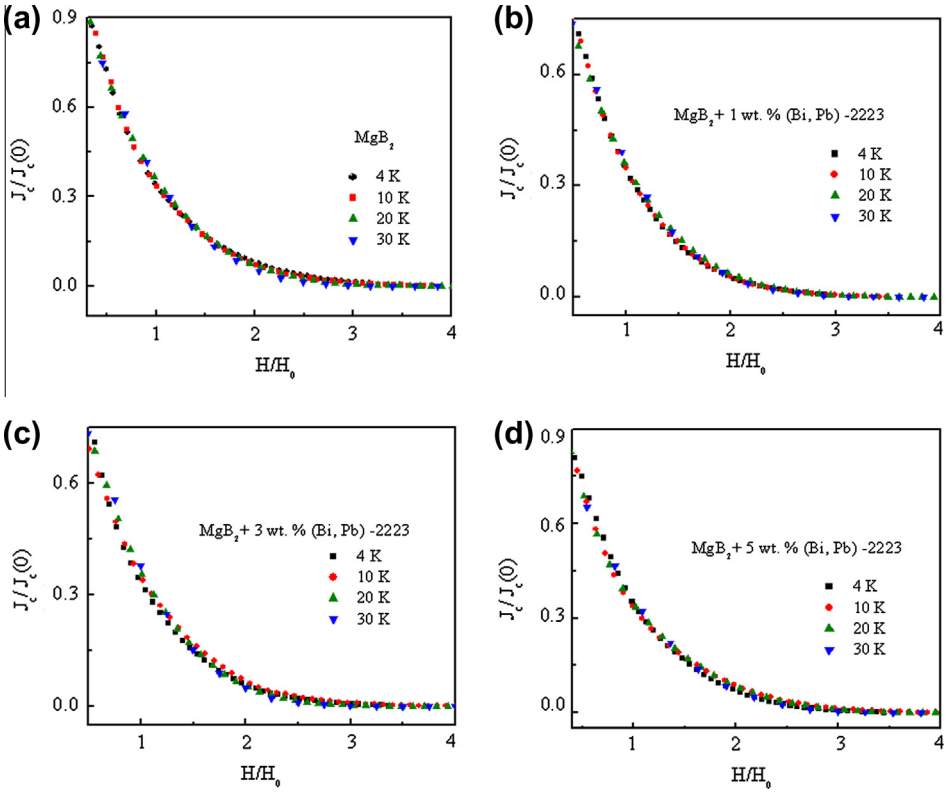

Fig. 10. Scaling behavior of $J_c/J_c(0)$ as a function of H/ H_0 for (a) MgB_2. (b) MgB_2 + 1 wt.% 2223. (c) MgB_2 + 3 wt.% 2223 and (d) MgB_2 + 5 wt.% 2223 samples at different temperatures.

interesting to note that the critical current density of the present series of 2223 added MgB_2 superconductors also display excellent scaling, if the best fitted parameters, viz., $J_c(0)$ and H_0 obtained from Eq. (6) are used as the normalization factors for critical current density (J_c) and field (H) respectively. It is clearly seen from Fig. 10(a–d) that the reduced critical current density, J_n (=J_c/J_c (0)) for both undoped MgB_2 and 2223 added MgB_2 pellets at different temperatures display an excellent scaling as a function of the reduced field h_n (=H/H_0).

The vortex-pinning (VP) interaction in type-II superconductors arises due to periodic variation of order parameter $|\psi(r)|^2$ or the local field $h(r)$, which can be separated into two different type of coupling mechanisms, viz., magnetic and core VP-interaction [48]. Out of these two coupling mechanisms, core interaction is more effective as compared to magnetic interaction for type-II superconductors and arises due to coupling between locally distorted superconducting properties and periodic variation of the superconducting order parameter. Depending upon type of inhomogeneity, core interaction is further classified in two types of pinning mechanisms [48]; one originates from the spatial variations in the density, elasticity or pairing interaction (viz., δT_c – type pinning) and the other originates from the variations in electron mean free path due to defects in the crystal lattice (viz., δl – type pinning) respectively. It may be noted that although δT_c – type pinning is known to be more dominant in pure MgB_2, the situation is not yet known for 2223 added MgB_2 samples. Ghorbani et al. [49] separated the contribution of both the mechanisms for their silicon oil doped MgB_2 system and to that end they expressed the crossover field at reduced temperature (t) as:

$$H_{sb}(t) = P_1 H_{sb}^{T_c} + P_2 H_{sb}^{l} \tag{7}$$

where, P_1 and P_2 are fitting parameters with the condition $P_1 + P_2 = 1$ and they denote the contribution of δT_c and δl type pinning respectively. The crossover fields, $H_{sb}^{T_c}$ and H_{sb}^{l} at reduced temperature t (=T/T_c) corresponding to δT_c and δl type pinning are defined as [42]:

$$H_{sb}^{T_c} = H_{sb}(0)\left(\frac{1-t^2}{1+t^2}\right)^{0.67} \quad \text{and} \quad H_{sb}^{l} = H_{sb}(0)\left(\frac{1-t^2}{1+t^2}\right)^{2} \tag{8}$$

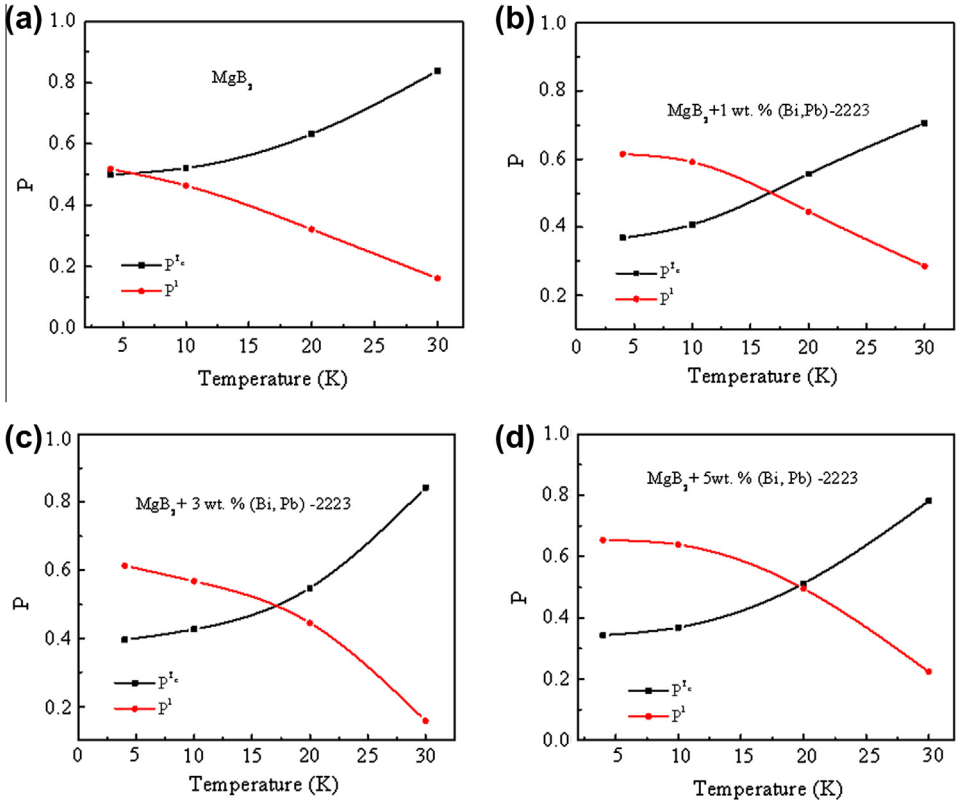

Fig. 11. Contribution of δT_c and δl type of pinning as a function of temperature for (a) MgB_2; (b) MgB_2 + 1 wt.% 2223; (c) MgB_2 + 3 wt.% 2223 and (d) MgB_2 + 5 wt.% 2223 samples.

In Eq. (8), $H_{sb}(0)$ is the crossover field at 0 K. Substituting for $H_{sb}^{T_c}$ and H_{sb}^{l} in Eq. (7), one gets:

$$H_{sb} = H_{sb}(0)\left[P_1\left(\frac{1-t^2}{1+t^2}\right)^{0.67} + (1-P_1)\left(\frac{1-t^2}{1+t^2}\right)^{2}\right] \quad (9)$$

To investigate the pinning mechanisms associated with pure and 2223 added MgB_2 pellets at different temperatures, the crossover field $H_{sb}(t)$ is fitted with Eq. (9), taking $H_{sb}(0)$ and P_1 as free parameters (Fig. 9b) and the best fitted values are listed in Table 4. In order to compare the effect of δT_c and δl pinning, their relative contributions at different temperatures for the present set of samples are calculated from: $P^{T_c} = P_1 H_{sb}^{T_c}/H_{sb}$, and $P^{l} = P_2 H_{sb}^{l}/H_{sb}$ respectively and are plotted in Fig. 11(a–d). Fig. 11a clearly shows the dominance of δT_c pinning for MgB_2 above 4 K, which is consistent with the earlier report [42]. On the other hand, for 2223 added MgB_2, δl pinning appears to dominate at low temperatures and enhances with increased 2223 concentration in MgB_2 (Fig. 11(b–d)). The dominance of δl type pinning for 2223 added MgB_2 is supported by the fact that 2223 addition in MgB_2 causes shortening of the mean free path. The dominance of δl pinning diminishes with increasing temperatures and at certain temperature both the pinning have nearly equal dominance. However, above this temperature, δT_c pinning mechanism becomes more important.

4. Conclusions

Effect of addition of superconducting 2223 on the structural and superconducting properties of polycrystalline MgB_2 is discussed. Structural analysis indicates absence of any substitution for both Mg and B, due to 2223 addition. Morphological features of 2223 added MgB_2 pellets display presence of 2223 grains or clusters at the grain boundary. Superconducting transition temperatures (T_{C0}) of MgB_2 polycrystals remain practically unaltered with addition of 2223, which is similar to that reported for both YBCO and 2212 added MgB_2. Temperature dependence of the normal state electrical resistivity of 2223 added MgB_2 superconductors is explained well in terms of modified Rowell's model. Critical current density of MgB_2 containing 1 wt.% of 2223 display nearly 2 times enhancement over the entire field range between 0 and ±6 T, however, for higher 2223 content in MgB_2, substantial drop in J_C over the entire field range is observed. The field dependence of J_C of 2223 added MgB_2 show excellent correspondence only in terms of '*collective pinning model*'. We further establish that the critical current density of 2223 added MgB_2 display excellent scaling in terms of the reduced current density (J_c/J_c (0)) and the reduced field (H/H_0), where, J_c (0) and H_0 are the parameters obtained from collective pinning model. For pure MgB_2, δTc type pinning is identified as main pinning mechanism, while at low temperature, δl type pinning dominates in 2223 added MgB_2 superconductors.

References

[1] J. Nagamatsu, N. Nakagawa, T. Muranaka, Y. Zenitani, J. Akimitsu, Nature 410 (2001) 63–64.
[2] Y. Zhang, S.H. Zhou, X.L. Wang, S.X. Dou, Physica C 468 (2008) 1383–1386.
[3] G. Yuan, X. Xu, Z. Wang, D. Lu, X. Jin, Solid State Commun. 135 (2005) 352–355.
[4] S.X. Dou, S. Soltanian, J. Horvat, X.L. Wang, S.H. Zhou, M. Ionescu, H.K. Liu, Appl. Phys. Lett. 81 (2002) 3419–3421.
[5] K. Shinohara, H. Ikeda, R. Yoshizaki, Physica C 463–465 (2007) 471–473.
[6] N. Chikumoto, A. Yamamoto, M. Konczykowski, M. Murakami, Physica C 388–389 (2003) 167–168.
[7] S. Okayasu, M. Sasase, K. Hojou, Y. Chimi, A. Iwase, H. Ikeda, R. Yoshizaki, T. Kamabara, H. Sato, Y. Hamatani, A. Maeda, Physica C 382 (2002) 104–107.
[8] G. Serrano, A. Serquis, D. Rodrigues Jr., M.T. Malachevsky, J.M. Espasandin, C. Ayala, J. Phys. Conf. Ser. 97 (2008) 0121271–0121277.
[9] S.X. Dou, S. Soltanian, W.K. Yeoh, Y. Zhang, IEEE Trans. Appl. Supercond. 15 (2005) 3219–3222.

[10] E.H. Brandt, Rep. Prog. Phys. 58 (1995) 1465–1594.
[11] X.F. Rui, X.F. Sun, X.L. Xu, L. Zhang, H. Zhang, Int. J. Mod Phys B 19 (2005) 375–377.
[12] Y.Y. Xu, J. Ren, S.H. Han, H. Zhang, Int. J. Mod Phys B 21 (2007) 3352–3354.
[13] T.M. Shen, G. Li, X.T. Zhu, C.H. Cheng, Y. Zhao, Supercond. Sci. Technol. 18 (2005) L49–L52.
[14] E.H. Brandt, Phys. Status Solidi B 71 (1975) 277–291.
[15] E.V. Thuneberg, J. Low Temp. Phys. 62 (1986) 27–37.
[16] K. Vinod, N. Varghese, R.G. Abhilash, U. Symaprasad, S.B. Roy, J. Alloys Comp. 464 (2008) 33–37.
[17] O.V. Shcherbakova, A.V. Pan, J.L. Wang, A.V. Shcherbakov, S.X. Dou, D. Wexler, E. Babic, M. Jercinovic, O. Husnjak, Supercond. Sci. Technol. 21 (2008) 0150051–0150057.
[18] Q. Cai, Y. Liu, Z. Ma, L. Yu, Physica C 496 (2014) 53–57.
[19] Y. Takikawa, M. Takeda, M. Migita, M. Uehara, T. Kuramoto, Y. Kimishima, Physica C 471 (2011) 905–907.
[20] W. Zhu, P.S. Nicholson, J. Appl. Phys. 73 (1993) 8423–8428.
[21] P. Lezza, C. Senatore, R. Flukiger, Supercond. Sci. Technol. 19 (2006) 1030–1033.
[22] E. Aksu, J. Alloys Comp. 552 (2013) 376–381.
[23] V. Singh, P. Chauhan, J. Phys. Chem. Solids 70 (2009) 1074–1079.
[24] E. Bayazit, S. Altin, M.E. Yakinci, M.A. Aksan, Y. Balci, J. Alloys Comp. 457 (2008) 42–46.
[25] J.M. Rowell, Supercond. Sci. Technol. 16 (2003) R17–R27.
[26] M.A. Susner, M. Bhatia, M.D. Sumption, E.W. Collings, J. Appl. Phys. 105 (2009) 1039161–1039167.
[27] M. Eisterer, J. Emhofer, S. Sorta, M. Zehetmayer, H.W. Weber, Supercond. Sci. Technol. 22 (2009) 0340161–0340167.
[28] N. Novosel, D. Pajic, Z. Skoko, M. Mustapic, E. Babic, K. Zadroa, J. Horvat, Phys. Proced. 36 (2012) 1498–1503.
[29] V. Chabanenko, R. Puzniak, A. Nabialek, S. Vasiliev, V. Rusakov, L. Huanqian, R. Szymczak, H. Szymczak, J. Jun, J. Karpinski, V. Finkel, J. Low Temp. Phys. 130 (2003) 175–191.
[30] C.P. Bean, Phys. Rev. Lett. 8 (1962) 250–253.
[31] A. Vajpayee, V.P.S. Awana, S. Yu, G.L. Bhalla, H. Kishan, Physica C 470 (2010) S653–S654.
[32] Z. Zhang, H. Suo, L. Ma, T. Zhang, M. Liu, M. Zhou, Physica C 471 (2011) 908–911.
[33] T. Harada, K. Yoshida, Physica C 383 (2002) 48–54.
[34] V. Sandu, Mod. Phys. Lett. B 26 (2012) 12300071–123000718.
[35] D.C. Larbalestier, L.D. Cooley, M.O. Rikel, A.A. Polyanskii, J. Jiang, S. Patnaik, X.Y. Cai, D.M. Feldmann, A. Gurevich, A.A. Squitieri, M.T. Naus, C.B. Eom, E.E. Hellstrom, R.J. Cava, K.A. Regan, N. Rogado, M.A. Hayward, T. He, J.S. Slusky, P. Khalifah, K. Inumaru, M. Haas, Nature 410 (2001) 186–189 (London).
[36] E.J. Kramer, J. Appl. Phys. 44 (1973) 1360–1370.
[37] Y. Zhao, C.H. Cheng, X.F. Rui, H. Zhang, P. Munroe, H.M. Zeng, N. Koshizuka, M. Murakami, Appl. Phys. Lett. 83 (2003) 2916–2918.
[38] J. Wang, Z.X. Shi, H. Lv, T. Tamegai, Physica C 445–448 (2006) 462–465.
[39] J. Horvat, S. Soltanian, A.V. Pan, X.L. Wang, J. Appl. Phys. 96 (2004) 4342–4351.
[40] G. Blatter, M.Y. Feigelman, Y.B. Geshkenbein, A.I. Larkin, V.M. Vinokur, Rev. Mod. Phys. 66 (1994) 1125–1388.
[41] Sudesh, N. Kumar, S. Das, C. Bernhard, G.D. Varma, Supercond. Sci. Technol. 26 (2013) 0950081–0950088.
[42] M.J. Qin, X.L. Wang, H.K. Liu, S.X. Dou, Phys. Rev. B 65 (2002) 1325081–1325084.
[43] J.L. Wang, R. Zeng, J.H. Kim, L. Lu, S.X. Dou, Phys. Rev. B 77 (2008) 174501.
[44] A.F. Salem, K.A. Ziq, A.A. Bahgat, J. Supercond. Nov. Magn. 26 (2013) 1517–1520.
[45] D. Tripathi, T.K. Dey, J. Supercond. Nov. Magn. (2014), http://dx.doi.org/10.1007/s10948-014-2508-1.
[46] T. Higuchi, S.I. Yoo, M. Murakami, Phys. Rev. B 59 (1999) 1514–1527.
[47] Kh.A. Ziq, P.C. Canfield, J.E. Ostenson, D.K. Finnemore, Phys. Rev. B 60 (1999) 3603–3607.
[48] R. Wordenweber, Rep. Prog. Phys. 62 (1999) 187–236.
[49] S.R. Ghorbani, X.L. Wang, S.X. Dou, S. Lee, M.S.A. Hossain, Phys. Rev. B 78 (2008) 1845021–1845025.